A Theoretical Evaluation of Rigid Baffles in Suppression of Combustion Instability

by

M. R. Baer - Sandia Laboratories,
Albuquerque, New Mexico

and

C. E. Mitchell - Colorado State University
Ft. Collins, Colorado

*** This work was supported by a NASA Grant No. NGR-06-002-095.

A THEORETICAL EVALUATION OF RIGID BAFFLES IN SUPPRESSION OF COMBUSTION INSTABILITY

By

M. R. Baer and C. E. Mitchell

September 13, 1976

Backup Document for AIAA Synoptic Scheduled for Publication in the AIAA Journal, February 1977

Sandia Laboratories
Aerothermodynamic Division 1333
Albuquerque, New Mexico 87115

ABSTRACT

An analytical technique for the prediction of the effects of rigid baffles on the stability of liquid propellant combustors is presented. This analysis employs a three dimensional combustor model characterized by a concentrated combustion source at the chamber injector and a constant Mach number nozzle. An eigenfunction-matching method is used to solve the linearized partial differential equations describing the unsteady flow field. Boundary layer corrections to this unsteady flow are used in a mechanical energy dissipation model to evaluate viscous and turbulence effects within the flow. An integral stability relationship is then employed to predict the decay rate of the oscillations.

Results of this analysis agree qualitatively with experimental observations and show that sufficient dissipation exists to indicate that the proper mechanism of baffle damping is a fluid dynamic loss. The response of the dissipation model to varying baffle blade length, mean flow Mach number and oscillation amplitude is examined.

Nomenclature

a^*	speed of sound
$A_{\ell m}^{\mu}$	coefficient matrix for velocity potential in baffle compartment
$B_{\ell m}$	coefficient matrix for velocity potential in main chamber
E_{dis}	mechanical energy dissipation
i	unit complex
J_m	bessel function of first kind of order m
$L = L^*/R^*$	chamber length
$\dot{m} = \dot{m}^*/\bar{\rho}^*\bar{a}^*R^{*2}$	mass generation rate
M	steady state mach number
n	interaction index
N	total number of baffle compartments
$P = P^*/\bar{P}^*$	pressure
$\vec{q} = \vec{q}^*/\bar{a}^*$	velocity
$r = r^*/R^*$	radial coordinate
R^*	chamber radius
$S = S^*/R^{*2}$	surface area
$T_B = T_B^*/R^*$	baffle blade thickness
$t = t^*\bar{a}^*/R^*$	time
$U = U^*/\bar{a}^*$	boundary layer edge velocity
$z = z^*/R^*$	axial coordinate
$z_B = z_B^*/R^*$	baffle blade length
α	circumferential coordinable at baffle blade tip

γ	ratio of specific heats
ε	wave amplitude
$\eta = \eta^*/R^*$	coordinate normal to surface covered by boundary layer
θ	circumferential coordinate
$\lambda = \lambda^* R^*/\bar{a}^*$	decay rate
$\lambda_{\ell m}^{B}$	ℓth root of $\frac{d}{dr}\left[\frac{J_{mN}}{2}\left(\lambda_{\ell m}^{B} r\right)\right] = 0$ at $r = 1$
$\lambda_{\ell m}^{C}$	ℓth root of $\frac{d}{dr}\left[J_m\left(\lambda_{\ell m}^{C} r\right)\right] = 0$ at $r = 1$
$\mu_\nu = \mu_\nu^*/\bar{\rho}^*\bar{a}^*R^*$	viscosity coefficient
$\rho = \rho^*/\bar{\rho}^*$	density
$\bar{\tau} = \bar{\tau}^* \bar{a}^*/R^*$	time lag
ϕ	velocity potential
ψ	stream function
$\omega = \omega^* R^*/\bar{a}^*$	complex frequency
$\zeta = \zeta^*/R^*$	radial coordinate near baffle blade tips
$\delta_{m,\hat{m}}$	kronecker delta

Subscripts

B	baffle quantity
C	main chamber quantity
R	real part

Superscripts

B	baffle quantity
C	main chamber quantity
$\bar{}$	steady state quantity
*	dimensional quantity
^	designates a particular mode
'	perturbation quantity

Mathematical Symbols

$\overline{\quad}$	complex conjugate
$\langle\ \rangle$	time average
$O(\ )$	order
$\frac{D}{Dt}(\ ) = \frac{\partial}{\partial t} + \vec{q} \cdot \vec{\nabla}$	total derivative

INTRODUCTION

Increased liquid propellant combustor performance has necessitated the use of highly energetic propellants and injector designs that promote more efficient combustion. These influences tend to encourage the likelihood of the phenomena termed combustion instability. Instead of altering these combustion characteristics, mechanical damping devices have often been incorporated in combustor designs. Two such devices have been successfully used to suppress instability.

One of these devices is the acoustic liner which is a series of Helmholtz resonators or circumferential slots that are placed or machined on the periphery of the chamber. Jet losses are primarily responsible for the damping that is produced by this device. Experimental verification of this mechanism has been established[1] and a strong theoretical basis for design of these devices has been established in several combustion instability analyses.[2,3] However, designers are reluctant to use this mechanical damping device because it creates local hot spots on the chamber walls and heat transfer becomes an important consideration.

The other device is termed a baffle. The baffle was first proposed in 1954[4] and consists of a series of blades attached to the injector surface protruding axially down the chamber. Several baffle configurations have been conceived by designers particularly with respect to blade arrangement and blade

shape. However, utilizing these designs requires expensive and time consuming full scale tests. Heat transfer aspects of this device are also of importance but because the baffle is an internal device separable from the combustor walls these considerations aren't critical as far as the structural integrity of the chamber is concerned.

Sufficient experimental verification[5] of the stability improvement of combustors with baffles has been produced, however total reliability of this device has been limited since a few combustors have failed to gain stability improvement with the addition of a baffle.[6] A theoretical treatment of baffle damping is needed to avoid these anomalies and aid in design. Unfortunately, no satisfactory theory exists and design of the baffle has remained a black art which utilizes several empirical rules that may or may not be applied effectively in a particular engine configuration.

The purpose of this work is to investigate a possible fluid dynamic mechanism for the damping produced by baffles. An analytical model incorporating viscous and turbulence effects is then to be used in a stability evaluation of baffled combustors which are modeled with a concentrated combustion source at the injector and a short nozzle.

THEORY

Three dimensional small amplitude oscillations are studied in a combustor modeled as a right circular cylinder. The baffles

enter the problem as discontinuities which rigidly protrude axially downstream of the injector end of the chamber. The chamber is then split into multiple equal angle sector compartments which are terminated at the baffle ends by a single main chamber (refer to Figure 1).

Combustion and nozzle influences enter the problem as gain-loss boundary conditions. The combustion is assumed to be concentrated at the injector face. Support for this assumption is based upon experimental observation that the majority of the combustion processes are frequently completed very near the injector of the chamber. This model for the combustion also overestimates the energy input to the flow and thus represents the worst condition for stability.[7] The unsteady model for combustion mass generation used here is assumed to be only pressure dependent according to the Crocco n - τ lag theory.[8]

At the opposite end of the chamber is a "short", quasi-steady nozzle. Due to the restrictive nature of the flow within this nozzle, a constant Mach number condition exists at its entrance. The choice of this type of nozzle is made for simplicity in this analysis. The effects of finite length nozzles on three dimensional linear oscillations have been well studied[9] and are not critical to the baffle damping mechanism proposed.

Periodic oscillations are treated for a thermally and calorically perfect gaseous flow. The concentrated combustion assumption permits the gas dynamic flow field to be represented as a single constituent, product gas with no heat transfer or diffusion processes taking place. The core flow within the chamber is charac-

terized by a constant Mach number steady flow and is assumed to be irrotational. Consequently it is consistent to assume a velocity potential exists for the core main flow. Corrections to these assumptions are made by making boundary layer adjustments at the appropriate surfaces.

One final assumption is made with regard to this solution. Entropy variations are neglected in this analysis. This assumption is consistent with the small overall influence they produce on the problem.[10]

Before mathematically describing the preceding flow, a nondimensionalization of the thermodynamic variables and the velocity field with respect to their steady state values is made. Because of the concentrated combustion assumption, the steady state thermodynamic variables and gas velocity are spatially independent and are represented as constants.

The nondimensional conservation equations governing the flow are given by the following relationships.

Conservation of Mass:

$$\frac{D\rho}{Dt} + \rho\vec{\nabla} \cdot \vec{q} = 0$$

Conservation of Momentum:

$$\rho \frac{D\vec{q}}{Dt} + \frac{1}{\gamma} \vec{\nabla} P = 0$$

Homentropic Condition:

$$P = \rho^{\gamma}$$

The velocity potential assumption allows the velocity field to have the following representation:

$$\vec{q} = \vec{\nabla} \phi$$

The state variables are then represented as power series expansions in an amplitude parameter (ε), i.e.

$$\phi = \bar{\phi} + \varepsilon\phi' + O(\varepsilon^2)$$

$$P = 1 + \varepsilon P' + O(\varepsilon^2)$$

With these expansions a first order linearization of the conservation equations is made which yields the following equations:

$$P' = \gamma\rho'$$

$$\nabla^2\phi' - \frac{\partial^2\phi'}{\partial t^2} = 2M \frac{\partial^2\phi'}{\partial z \partial t} + M^2 \frac{\partial^2\phi'}{\partial z^2} \qquad (1)$$

$$P' = - \gamma \left[\frac{\partial\phi'}{\partial t} + M \frac{\partial\phi'}{\partial z}\right] \qquad (2)$$

Since standing and traveling wave solutions are examined in this analysis, it is consistent to assume exponential time dependence of the perturbations. The perturbed pressure and velocity potential thus have the forms:

$$P' = P(\vec{R})\, e^{i\omega t} \text{ and } \phi' = \phi(\vec{R})\, e^{i\omega t}$$

where $\omega = \omega_r + i\lambda$ is the complex frequency and λ is the decay rate. Substitution of this time dependence transforms equations 1 and 2 into the following forms:

$$\nabla^2\phi + \omega^2\phi = 2i\omega M \frac{\partial\phi}{\partial z} + M^2 \frac{\partial^2\phi}{\partial z^2} \tag{3}$$

$$P = -\gamma\left[i\omega\phi + M \frac{\partial\phi}{\partial z}\right] \tag{4}$$

The gain-loss boundary conditions at the injector and nozzle entrance surfaces are formulated, respectively, with the aid of Crocco's n - τ time lag theory and the "short" nozzle approximation. The combustion boundary condition is mathematically expressed as:

$$\dot{m}' = \bar{\dot{m}} n \left\{P'(t) - P'(t - \bar{\tau})\right\}$$

or

$$\left.\frac{\partial \phi}{\partial z}\right|_{z=0} + \left.\frac{MP}{\gamma}\right|_{z=0} = Mn(1 - e^{-i\omega\bar{\tau}})\ P\Big|_{z=0} \qquad (5)$$

where n is the interaction index, (a measure of the amplitude dependence of the mass generation on the pressure), and $\bar{\tau}$ is the sensitive time lag, (a time phasing of the mass generation with the pressure).

The "short" nozzle (constant entrance Mach number) approximation allows a loss boundary condition which is expressed mathematically as:

$$\left.\frac{\partial \phi}{\partial z}\right|_{z=L} = M\ \frac{(\gamma - 1)}{2\gamma}\ P\Big|_{z=L} \qquad (6)$$

On the remaining surfaces of the chamber and on the baffle blade surfaces hard wall boundary conditions are used. This is expressed by a zero normal component of velocity.

With the partial differential equation for the first order velocity potential and the linearized boundary conditions a solution is then obtained. Because of the discontinuous geometry of the problem, a separation of variables solution can not be directly obtained and a more sophisticated method is necessary. This method calls for separate solutions in the baffle cavities and the main chamber. A matching of these solutions is made at an artificial interface between these regions thus producing the complete solution.

The solution within the baffle cavities ($0 \leq z \leq z_B$) is found by separation of variables and utilizes the injector and hard wall boundary conditions. This solution takes the form:

$$\phi^{\mu} = \sum_{m=0}^{\infty} \sum_{\ell=1}^{\infty} A^{\mu}_{\ell m} \psi^{B}_{\ell m}(r,\theta) \left\{ \frac{e^{iB_{1,B}z} + C_B e^{iB_{2,B}z}}{e^{iB_{1,B}z_B} + C_B e^{iB_{2,B}z_B}} \right\} \tag{7}$$

where

$$\psi^{B}_{\ell m}(r,\theta) = \cos \frac{mN\theta}{2} J_{\frac{mN}{2}} \left(\lambda^{B}_{\ell m} r\right) \qquad \frac{2\pi}{N}(\mu-1) \leq \theta \leq \frac{2\pi\mu}{N}$$

$$B_{1,B} = \frac{\omega M + \left(\omega^2 M^2 + \left(M^2 - 1\right)\left(\lambda^{B^2}_{\ell m} - \omega^2\right)\right)^{1/2}}{\left(1 - M^2\right)}$$

$$B_{2,B} = \frac{\omega M - \left(\omega^2 M^2 + \left(M^2 - 1\right)\left(\lambda^{B^2}_{\ell m} - \omega^2\right)\right)^{1/2}}{\left(1 - M^2\right)}$$

$$C_B = - \left[\frac{B_{1,B} + M\left|\gamma n\left(1 - e^{-i\omega\bar{\tau}}\right) - 1\right|(\omega + B_{1,B})}{B_{2,B} + M\left|\gamma n\left(1 - e^{-i\omega\bar{\tau}}\right) - 1\right|(\omega + B_{2,B})} \right]$$

and N refers to the total number of baffle cavities.

Within the main chamber ($z_B \leq z \leq L$) the perturbed velocity potential takes the form

$$\phi^c = \sum_{m=0}^{\infty}\sum_{\ell=1}^{\infty} B_{\ell m}\Psi^c_{\ell m}(r,\theta)\left\{\frac{e^{iB_{1,c}(z-L)} + e^{iB_{2,c}(z-L)}}{e^{iB_{1,c}(z_B-L)} + C_c e^{iB_{2,c}(z_B-L)}}\right\} \tag{8}$$

where the standing wave solution is made by specifying:

$$\Psi^c_{\ell m}(r,\theta) = \text{Cos } m\theta\ J_m(\lambda^c_{\ell m} r)$$

and the traveling wave solution is given by:

$$\Psi^c_{\ell m}(r,\theta) = e^{im\theta} J_m(\lambda^c_{\ell m} r)$$

and

$$B_{1,c} = \frac{\omega M + \left(\omega^2 M^2 + (M^2 - 1)\left(\lambda^{c\,2}_{\ell m} - \omega^2\right)\right)^{1/2}}{(1 - M^2)}$$

$$B_{2,c} = \frac{\omega M + \left(\omega^2 M^2 + (M^2 - 1)\left(\lambda^{c\,2}_{\ell m} - \omega^2\right)\right)^{1/2}}{(1 - M^2)}$$

$$C_c = -\left[\frac{B_{1,c} + M(\gamma - 1)(\omega + B_{1,c})/2}{B_{2,c} + M(\gamma - 1)(\omega + B_{2,c})/2}\right]$$

The complete solution is then obtained by determining the proper set of $\{A^{\mu}_{\ell m}\}$ and $\{B_{\ell m}\}$. The continuity of axial velocity and velocity potential at the main chamber-baffle compartment interface produce the conditions necessary for the specification of the eigenfunction coefficients.

With the aid of the orthogonality properties of the series the following matching equations are obtained:

$$A^{\mu}_{\ell m} = \sum_{m'=0}^{\infty} \sum_{\ell'=1}^{\infty} B_{\ell' m'} \frac{\int_{\frac{2\pi}{N}(\mu-1)}^{\frac{2\pi\mu}{N}} \int_0^1 \psi^B_{\ell m}(r,\theta)\ \psi^C_{\ell' m'}(r,\theta)\ r dr d\theta}{\int_{\frac{2\pi}{N}(\mu-1)}^{\frac{2\pi\mu}{N}} \int_0^1 \psi^{B\,2}_{\ell m}(r,\theta)\ r dr d\theta} \tag{9}$$

and

$$B_{\ell' m'} \left\{ \frac{iB_{1,c} e^{iB_{1,c}(z_B - L)} + iB_{2,c} C_c e^{iB_{2,c}(z_B - L)}}{e^{iB_{1,c}(z_B - L)} + C_c e^{iB_{2,c}(z_B - L)}} \right\} =$$

$$\sum_{m=0}^{\infty} \sum_{\ell=1}^{\infty} \left\{ \frac{iB_{1,B} e^{iB_{1,B} z_B} + iB_{2,B} C_B e^{iB_{2,B} z_B}}{e^{iB_{1,B} z_B} + C_B e^{iB_{2,B} z_B}} \right\} X \tag{10}$$

$$\left\{ \sum_{\mu=1}^{N} A_{\ell m}^{\mu} \frac{\int_{\frac{2\pi}{N}(\mu-1)}^{\frac{2\pi\mu}{N}} \int_{0}^{1} \psi_{\ell m}^{B}(r,\theta)\ \overline{\psi_{\ell',m'}^{c}}(r,\theta)\ r\,dr\,d\theta}{\int_{0}^{2\pi} \int_{0}^{1} \psi_{\ell',m'}^{c}(r,\theta)\ \overline{\psi_{\ell',m'}^{c}}(r,\theta)\ r\,dr\,d\theta} \right\}$$

Equation 9 is the representation of the matching of velocity potential and Equation 10 is the matching of axial velocity at $z = z_B$. It is recognized that the solution to this problem satisfies a homogeneous differential equation with homogeneous boundary conditions and as such poses an eigenvalue problem. Since the amplitude is arbitrary in this solution, a normalization to a particular mode within the main chamber is made. This gives an additional relationship that is used to compute the eigenvalue (frequency). Mathematically this is expressed as:

$$B\hat{\hat{}}_{\ell m} = 1$$

or

$$\left(\frac{iB_{1,c} e^{iB_{1,c}(z_B-L)} + iB_{2,c} C_c e^{iB_{2,c}(z_B-L)}}{e^{iB_{1,c}(z_B-L)} + C_c e^{iB_{2,c}(z_B-L)}} \right) =$$

$$\sum_{m=0}^{\infty}\sum_{\ell=1}^{\infty}\left\{\frac{iB_{1,B}e^{iB_{1,B}z_B}+iB_{2,B}C_Be^{iB_{2,B}z_B}}{e^{iB_{1,B}z_B}+C_Be^{iB_{2,B}z_B}}\right\}X \tag{11}$$

$$\left\{\sum_{\mu=1}^{N}A_{\ell m}^{\mu}\frac{\int_{\frac{2\pi}{N}(\mu-1)}^{\frac{2\pi\mu}{N}}\int_0^1\psi_{\ell m}^{B}(r,\theta)\,\overline{\psi_{\hat{\ell}\hat{m}}^{C}(r,\theta)}\,r\,dr\,d\theta}{\int_0^{2\pi}\int_0^1\psi_{\hat{\ell}\hat{m}}^{C}(r,\theta)\,\overline{\psi_{\hat{\ell}\hat{m}}^{C}(r,\theta)}\,r\,dr\,d\theta}\right\}$$

where $\hat{m}$ and $\hat{\ell}$ respectively specifies the dominating transverse and radial modes in the main chamber.

A successive approximation technique is used to solve Equations 9, 10 and 11. The first approximation chosen for this method uses the unbaffled chamber velocity potential solution, i.e. $B_{\ell m} = \delta_{m,\hat{m}}\,\delta_{\ell,\hat{\ell}}$. With this approximation a calculation of the baffle compartment coefficients $\{A_{\ell m}^{\mu}\}$ is made using Equation 9. These coefficients, in turn, are used to recalculate the main chamber coefficients $\{B_{\ell m}\}$ from Equation 10 and the eigenvalue Equation 11. The procedure is then repeated until convergence is obtained. This iteration scheme converges very quickly and produces frequency predictions which have less than 5 percent differences after approximately 5 iterations.

In investigating the convergence of this solution, the matching relationships are checked by examining the velocity potential and axial velocity predictions at the interface $(z = z_B)$. With the use of Cesaro summation of the series expansions, // ← reasonable

agreement is obtained. Figure 2 depicts these matchings for a three compartment baffle configuration. This figure also indicates large unsteady gas velocities at the baffle blade tips ($z = z_B$) . In these regions the eigenfunction expansions fail to accurately represent the flow field.

It is therefore necessary to characterize the velocity field near the baffle blade tips using a different approach. To treat this problem a polar coordinate system is set up at the blade tips and an expansion of the velocity potential is obtained (refer to Figure 3 for the coordinate system).

If a proper ordering of the solution is made with respect to an asymptotic form, i.e.

$$\phi = \zeta^s A(\alpha) + K$$

where $0 \leqslant \zeta << 1$ and $s \geqslant 0$, it is found that the mean flow corrections to Equation 3 are of the orders $O(\zeta M)$ and $O(M^2)$. Also the $\omega^2\phi$ term in Equation 3 is a term of $O(\zeta^2)$. These terms are very small and are neglected to produce the asymptotic solution:

$$\phi = a\zeta^{1/2}\cos\alpha/2 + K + O(\zeta) \qquad \zeta << 1 \qquad (12)$$

This solution indicates the singular behavior of the velocity field, i.e. $\partial\phi/\partial\zeta \to \infty$ and $1/\zeta\ \partial\phi/\partial\alpha \to \infty$; $\zeta \to o$. The constants a and

K are determined by matching this asymptotic solution at some ζ_c with the outer eigenfunction expansions. Matching is required at two values of α for the fixed radius, ζ_c. The α values are chosen to produce the best overall angular match with the eigenfunction solution. Proper choice of ζ_c is made so that a region of proper matching with the outer expansions is realized.

With this representation of the strong flow near the baffle tips serving as the outer inviscid flow model, a calculation of energy dissipation due to molecular viscosity and turbulence in the boundary layer on the baffle blades is then made. Boundary layer predictions of the velocity profile are necessary. This prediction for a laminar, periodic flow is given as[12]:

$$U(\vec{R},t) = U(\eta = \delta,t)(1 - e^{-S_o\eta}) \tag{13}$$

$$S_o = (1 + i)\left(\omega/2\mu_\nu\right)^{1/2}$$

where $U(\eta = \delta,t)$ is the periodic outer flow transverse velocity given by the combined asymptotic-eigenfunction expansion solution and η is the normal component to the boundary surface (refer to Figure 4).

An estimate of the mechanical energy dissipation within the boundary layer volume is then calculated from the following integral[13]:

$$E_{dis} \cong \int_{V_{B.L.}} \mu_\nu\left(\frac{\partial U}{\partial \eta}\right)^2 d\eta dS \cong \gamma \int_S \left(\frac{\mu_\nu \omega}{2}\right)^{1/2} U^2(\eta = \delta,t)\, dS \tag{14}$$

Steady flow corrections are neglected in this calculation since these corrections are an order of magnitude smaller than the unsteady flow velocities. The second order influence of acoustic streaming is also neglected in the dissipation calculation. These corrections will increase the energy dissipation so the model gives a conservative estimate.

A time average of the above relationship will then physically represent an average quantity of mechanical energy that is transformed irreversibly into heat.

With the presence of combustion a highly turbulent flow situation must be realized and the existence of turbulence produces more energy dissipation[14] ← To account for this dissipation, the Boussinesq approximation is invoked which uses a stress-strain law for the time averaged turbulent flow. A "turbulent viscosity" which is a function of the local flow conditions is then necessary for the model. Many relationships exist for this parameter, each having limited applicability.[15] ← These relationships require a steady flow (apart from the turbulent fluctuations) far from the boundary surface. Models incorporating unsteady outer flow are nonexistent and must be created from existing steady flow theories. An effective viscosity model created by Spalding[16] is used for this analysis. This model is chosen because of its simplicity and its qualitative accuracy with respect to other combustion flow problems.[17] ← This model gives a representation of μ^*_{eff} as:

$$\mu^*_{eff} \propto \rho^{*2/3}\left(\dot{m}^*_F U^{*2}_F + \dot{m}_0 U^{*2}_0\right)^{1/3}$$

where the F and 0 subscripts refer to the fuel and oxidizer quantities. In order to be consistent with the single component gas assumption of this problem, the fuel and oxidizer velocities are assumed to be representable by the product gas velocity, i.e. $U^*_F \simeq U^*_0 \simeq U$. The equation for μ^*_{eff} then reduces to:

$$\mu^*_{eff} \propto \rho^* |U^*|$$

where $|U^*|$ is a r.m.s. value of speed in the entire turbulent field.

An incorporation of the periodic flow velocity into the model is then made by time averaging the r.m.s. $|U^*|$ to give the final form of μ_{eff}:

$$\mu_{eff} = C_{turb}\left\{M^2 + \varepsilon^2 \frac{\overline{U'U'}}{2}\right\}^{1/2} \qquad (15)$$

Geometrical corrections to this equation are neglected since they have a weak influence in the model. Spalding suggests a proportionality constant (C_{turb}) of the order 0(0.05).

This model is then used to calculate the turbulent dissipation. By assuming that the turbulent velocity profiles are similar to the laminar predictions given by Equation 13, the following integral relation for the dissipation is obtained:[18]

$$E_{dis}^{T} \cong \int_{S_B} \gamma \left(\frac{\mu_{eff}\omega}{2} \right)^{1/2} U^2 dS \qquad (16)$$

The importance of the exactness of the turbulent velocity profile is secondary since a global, integral quantity is evaluated. However, it is experimentally observed that turbulent profiles are steeper in shape than the laminar flow profiles and consequently this dissipation calculation could be underestimated.

One final correction is necessary for the dissipation calculation. A physically impossible infinitely thin baffle blade would create an infinite amount of energy loss because of the singular behavior of the velocity at the tip. A baffle blade of finite thickness will therefore be used in this problem.

To account for this thickness a neighboring streamline is used to represent the baffle surfaces. This eliminates a reworking of the solution to correct for the baffle shape since the normal component of velocity vanishes along a streamline. Near the tips of the blades the streamlines are well represented by $\psi = \zeta^{1/2} \mathrm{Sin}\alpha/2$ particularly for $\zeta << 1$ and $\pi/2 \leq \alpha \leq 3\pi/2$. This range defines the geometry of the blade tips.# This streamfunction is retained to describe the rest of the baffle blade surface but because the velocity decreases substantially away from the blade tips this surface description is of secondary importance in the dissipation calculation. Mathematically this surface is represented as:

Note that this assumption causes the tips to have a rounded profile, which is typical of the expected vortex flow region at the tip (See Figure 4).

$$\zeta^{1/2}\sin\alpha/2 = (T_B/4)^{1/2}$$

where T_B is the blade thickness.

A calculation of the tip loss is now possible using Equations 14, 15 and 16. Rather than correcting boundary conditions to account for this dissipation, as is done in acoustic theory, a more direct method of stability prediction is applied. An integral time average of the energy equation, derived by Cantrell and Hart,[19] is used to estimate the global stability of the flow within the combustor. Stability behavior (a calculation of decay rate of the perturbations) is examined by accounting for the energy inputs or extractions at the various surfaces of the chamber. Mathematically this relationship, correct to $0(\epsilon^2)$, is stated as:

$$2\lambda \left\langle \int_V \left\{ \frac{P'^2}{2\gamma} + \frac{\gamma}{2} \vec{q}' \cdot \vec{q}' + MU'P' \right\} dV \right\rangle$$

$$= \left\langle \oint_S \left\{ P'\vec{q}' + \frac{P'^2}{\gamma} M\vec{e}_k \right\} \cdot d\vec{S} \right\rangle \qquad (17)$$

where λ is the decay rate that is $0(\epsilon)$.

Evaluating the right-hand-side of the previous equation over the baffle surfaces results in a term representing the mechanical energy extracted at the surface. This can directly be equated to the dissipation integral Equation 16. By applying the appropriate boundary conditions, the Cantrell and Hart integral relationship has the final form:

$$\lambda = \left\{ -\int_{S_{inj}} \frac{Mn(1 - \cos\omega\bar{\tau})}{2} \overline{P'P'}\, dS_{inj} + \int_{S_{noz}} \frac{M(\gamma + 1)}{2\gamma} \frac{\overline{P'P'}}{2}\, dS_{noz} \right.$$

$$\left. + \int_{\gamma} \sqrt{\frac{\mu_{eff}\omega}{2}} \frac{\overline{U'U'}}{2}\, dS_B \right\} \Bigg/ \left\{ \int_V \left[\frac{\overline{P'P'}}{2\gamma} + \frac{\gamma}{2} \overline{\vec{q}'\vec{q}'} \right] dV \right\} \qquad (18)$$

The first term in the numerator represents the energy added to the unsteady flow by the combustion, the second term the energy extracted by the nozzle, and the third term the energy dissipated in the strong flow surrounding the baffle blade tips.

Stability calculations using this mathematical analysis were coded in Fortran and evaluated using a CDC 6400 computer. Inputs to the program include combustor geometry, baffle configuration, mean flow Mach number and oscillation mode character.

RESULTS

Previous investigations based on wave alteration as the possible mechanism for the damping produced by baffles have failed to correctly predict stability trends.[20,21] These studies have all neglected viscous and turbulence effects in the flow. The incorporation of these effects is of major importance in this problem and is necessary to describe the stability behavior of baffled combustors.

Linear stability predictions are examined in a particular chamber with a length to radius ratio of $L/R = 1.5$. A three bladed, evenly spaced baffle configuration with blade thickness $T_B = 0.05$ is used in the dissipation calculation. Three dimensional first transverse mode oscillations in the main chamber are studied with an unsteady combustion input which use $n = (\gamma + 1)/4\gamma$ and $\bar{\tau} = \pi/\lambda_{\ell m}^{\hat{}\hat{}}$. A neutrally stable unbaffled combustor is referenced with these parameters.

Before examining the stability trends, the effects of blade length on the normalized frequency, (frequency of the baffled chamber/frequency of the unbaffled chamber), are examined. Figure 5 shows that the frequency decreases when a baffle is added to a chamber. Furthermore, an increase in blade length further depresses the frequency. This prediction is in agreement with the experimental data provided by Aerojet-General.[20] It is also found that the normalized frequency is reduced with an increase in mean flow Mach number.

The principal result of these calculations is the prediction of combustor stability. Decay rates are calculated for various baffle blade lengths and chamber conditions. Decay in decibel/cycle is defined as follows:

$$\text{Decay in decibels/cycle} = 20 \log_{10} \left[\frac{P'(t)}{P'(t + 2\pi/\omega_r)} \right]$$

With the exponential time dependence of the oscillations in this problem this definition reduces to:

$$\text{Decay in decibels/cycle} = 54.575\lambda/\omega_r$$

where λ is the decay rate and ω_r is the frequency.

Decay rate predictions are shown in Figure 6 for a combustor with no mean flow and no combustion or nozzle influences. Two wave amplitudes, ($\varepsilon = 0.1$ and $\varepsilon = 0.2$), are shown in this figure and indicate the stabilizing behavior of baffles. It is also noted that the damping ability of the baffle improves with an increase in wave amplitude. This implies that the baffle is most effective in damping moderately large amplitude waves and that a baffle can be designed (in a conservative sense) with respect to a small amplitude theory.#

Figure 7 shows the stability prediction of a cylindrical combustor which has a mean flow ($M = 0.1$), combustion and nozzle influences and is experiencing oscillations with amplitude $\varepsilon = 0.1$.

It is also evident that this analysis is in the spirit of existing acoustic liner damping predictions in which nonlinear (amplitude dependent) damping mechanisms are combined with linear wave motion models.

Two types of oscillation are possible for this combustor: standing and traveling wave oscillations (refer to Figure 7). Without dissipation influences, it is seen that these solutions predict the same destabilizing influence for the baffle (consistent with the Rayleigh criterion[22]). With the inclusion of the mechanical energy dissipation in the model, these results are reversed and show a stabilizing influence for the baffle. It is seen that the traveling wave solution is most affected by the presence of the baffle and produces decay rates that are greater than those of the standing wave solution. This is a critical result because the traveling wave is most common and is the most destructive. It is also apparent that the phasing between the oscillations in the main chamber and the standing wave oscillations in the baffle cavities produce different stability results. This observation was made in Wieber's[5] experimental results.

Mean flow influence on decay rate is shown in Figure 8. This prediction indicates that a particular baffle blade length becomes less effective with an increase in mean flow Mach number, providing ε is constant. The Mach number dependence of ε due to combustion response has been neglected from this result and as such underpredicts the dissipation for large Mach numbers.

The sensitivity of turbulent viscosity model to the selection of C_{turb} is the final parameter examined in this study. Figure 9. shows that an increase in C_{turb} gives an increase in decay rate. This parameter has been treated as having secondary importance since only qualitative results can at this time be predicted.

More reliable turbulence data is necessary to assure the proper model for the turbulent viscosity or a proper value of C_{turb}.

CONCLUSIONS

A theoretical study of the stability of flows within combustion chambers with evenly spaced baffle configurations is examined. For the first time, a stabilizing influence for baffles has been properly predicted in an analytical model which incorporates the influences of a concentrated combustion source at the injector, a "short" nozzle terminating the chamber, and mechanical energy dissipation at the baffle blade tips. A summary of the results is as follows:

1. The addition of a baffle to a combustor in many situations will improve the stability of a chamber.
2. A fluid dynamic loss created by the effects of viscosity and turbulence comprise the damping mechanism of the baffle. This energy dissipation occurs locally at the baffle blade tips.
3. Without the effects of mechanical energy dissipation, wave alteration produced by the addition of a baffle to a combustor causes a destabilizing influence.
4. The baffle is most effective in damping the traveling transverse modes of oscillation.
5. The baffle is most effective in damping moderately large amplitude oscillations.

6. Longer baffles may be required for combustors which contain an increased mean flow.
7. The addition of a baffle to a combustion chamber depresses the oscillation frequency.
8. A linear theory may be effectively used in the design of a baffle.

REFERENCES

1. Zinn, B. T. (1972). Liner Damping Theory, In Harrje, D. T. and Reardon, F. H. (Eds.), Liquid Propellant Rocket Combustion Instability, NASA SP-194, pp. 400-410.

2. Tonon, T. S., Tang, P. K., Sirignano, W. A. and Harrje, D. T. (1971). Acoustic Liner Design from a Fluid Mechanis Approach, AIAA/SAE 7th Propulsion Joint Specialist Conference, AIAA paper No. 71-757.

3. Mitchell, C. E., Espander, W. R. and Baer, M. R. (1972). Determination of Decay Coefficients for Combustors with Acoustic Absorbers. NASA CR-120836.

4. Male, T. and Kerslake, W. R. (1954). A Method for Prevention of Screaming in Rocket Engines, NACA RM E54F28A.

5. Wieber, P. R. (1966). Acoustic Decay Coefficients of Simulated Rocket Combustors, NASA TN D-3425.

6. McBride, J. M. (1972). Baffle Blade Design. In Harrje, D. T. and Reardon, F. H. (Eds.), Liquid Propellant Rocket Combustion Instability, NASA SP194, pp. 395-399.

7. Baer, M. R., Mitchell, C. E. and Espander, W. R. (1974). Stability of Partially Lined Combustors with Distributed Combustion. AIAA Journal, Vol. 12, No. 4, pp. 475-480.

8. Crocco, L. and Cheng, S. I. (1956). Theory of Combustion Instability in Liquid Propellant Rocket Motors, AGARDograph No. 8, Butterworth, pp. 19-24.

9. Crocco, L. and Sirignano, W. A. (1966). Effect of the Transverse Velocity Component on the Nonlinear Behavior of Short Nozzles. AIAA Journal, Vol. 4, No. 8, pp. 1428-1430.

10. Mitchell, C. E. (1970). The Effect of Entropy Waves on High Frequency Pressure Oscillations in Liquid Rocket Motors, Combustion Science and Technology, Vol. 1, pp. 269-274.

11. Evans, C. M. (1970). Cesaro Summation of Series in Boundary-Value Problems. Journal of the Franklin Institute, Vol. 289, No. 3, pp. 185-191.

12. Schlichting H. (1968) Boundary Layer Theory, McGraw Hill Book Co., 6th Edition, pp. 411-427.

13. Landau, L. D. and Lifshitz, E. M. (1959), Fluid Mechanics, Pergamon Press, pp. 299-302.

14. Townsend, A. A., (1956) The Structure of Turbulent Shear Flow, Cambridge University Press, p. 43.

15. Launder, B. E. and Spalding, D. B. (1972). Mathematical Models of Turbulence, Academic Press, New York, Chapters 4, 5, 6.

16. Gosman, A. D., Pun, W. M., Runchel, A. K., Spalding, D. B. and Worfshtein, M. (1969). Heat and Mass Transfer in Recirculating Flows., Academic Press, New York, pp. 207-212.

17. Tou, P. R. and O'Hara, J. (1974). Experimental Determination of Turbulence in a GH_2-GOX Rocket Combustion Chamber. NASA CR-134672.

18. Schlichting, H. (1968). Boundary Layer Theory, McGraw Hill Book Co., 6th Edition, pp. 659.

19. Cantrell, R. H. and Hart, R. W. (1964). Interaction Between Sound and Flow in Acoustic Cavities: Mass, Momentum and Energy Considerations. Journal of Acoustical Society of America, Vol. 36, No. 4, pp. 697-706.

20. Reardon, F. H. (1972). Injector-face Baffles. In Harrje, D. T. and Reardon, F. H. (Eds.), Liquid Propellant Rocket Combustion Instability, NASA SP194, pp. 156-159.

21. Oberg C. L., Evers, W. H. and Wong, T. L. (1971). Analysis of the Wave Motion in Baffled Combustion Chambers. NASA CR-72879.

22. Rayleight, J. W. S. (1878). Nature, Vol. 18, pp. 319.

Figure Subheadings:

Figure 1. The geometry of the baffled combustion chamber
Figure 2. The axial velocity and velocity potential at the main chamber-baffle interface, (and r = 1), in a chamber with a three compartment baffle of length $z_B = 0.3$.
Figure 3. The polar coordinate system at the baffle blade tips.
Figure 4. The unsteady boundary layer over the baffle blades.
Figure 5. Normalized frequency vs. baffle blade length (z_B).
Figure 6. The effect of wave amplitude on decay in decibels/cycle vs. baffle blade length.
Figure 7. The standing and traveling wave predictions of decay/cycle vs. baffle blade length.
Figure 8. Mean flow Mach number effect on decay in decibels/cycle vs. baffle blade length (wave amplitude $\epsilon = 0.1$)
Figure 9. The effect of the turbulence coefficient (C_{turb}) on the stability predictions.

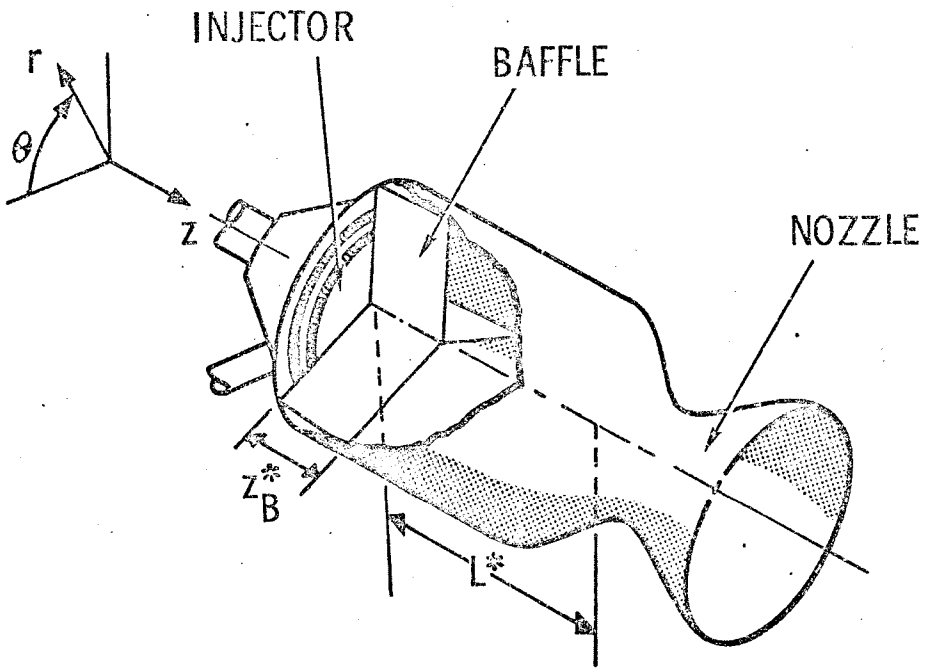
INJECTOR
BAFFLE
NOZZLE
r
θ
z
z^*_B
L^*

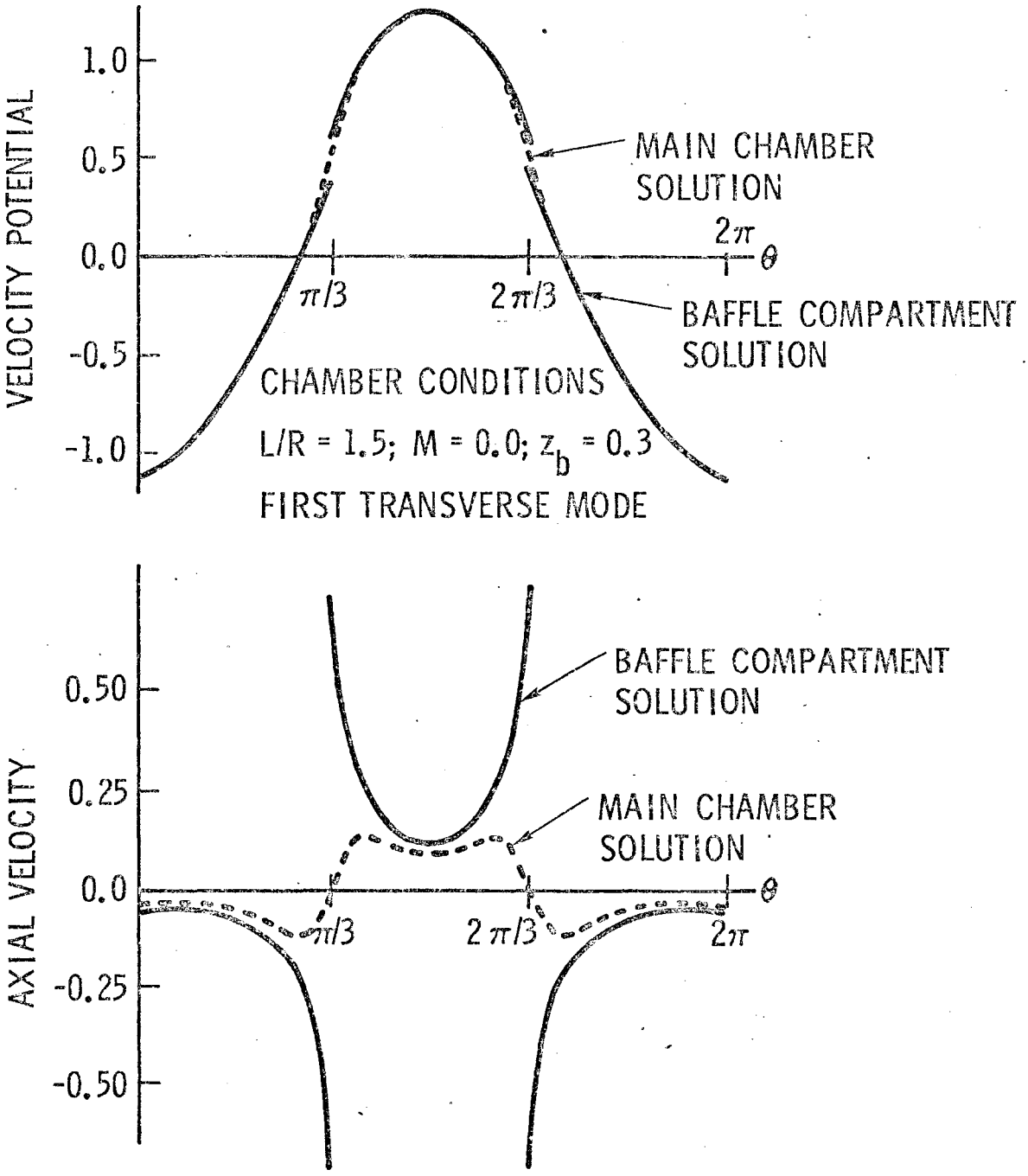
VELOCITY POTENTIAL
1.0
0.5
0.0
-0.5
-1.0
π/3
2π/3
2π
θ
MAIN CHAMBER SOLUTION
BAFFLE COMPARTMENT SOLUTION
CHAMBER CONDITIONS
L/R = 1.5; M = 0.0; z_b = 0.3
FIRST TRANSVERSE MODE
AXIAL VELOCITY
0.50
0.25
0.0
-0.25
-0.50
π/3
2π/3
2π
θ
BAFFLE COMPARTMENT SOLUTION
MAIN CHAMBER SOLUTION

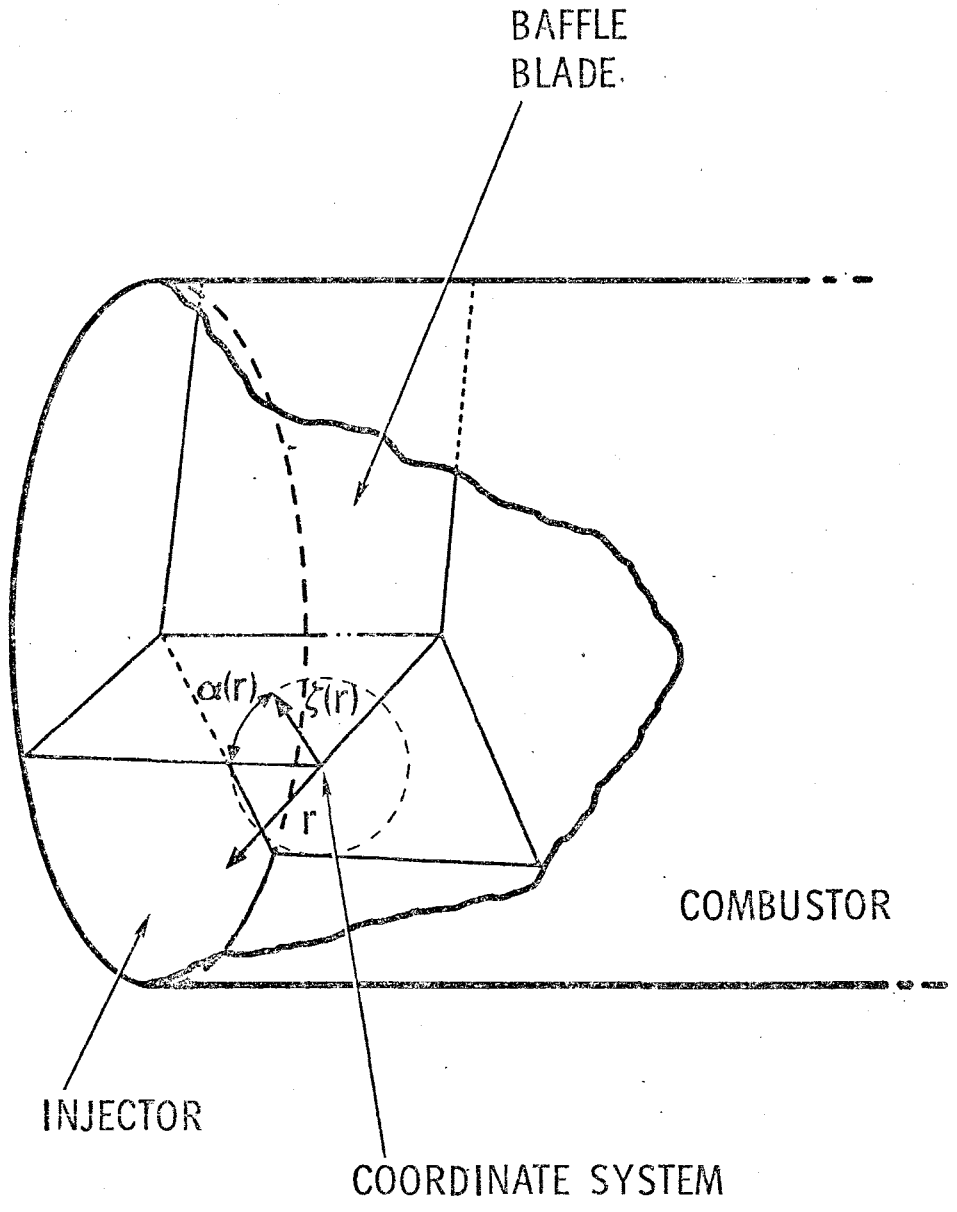
BAFFLE
BLADE
α(r)
ζ(r)
r
COMBUSTOR
INJECTOR
COORDINATE SYSTEM

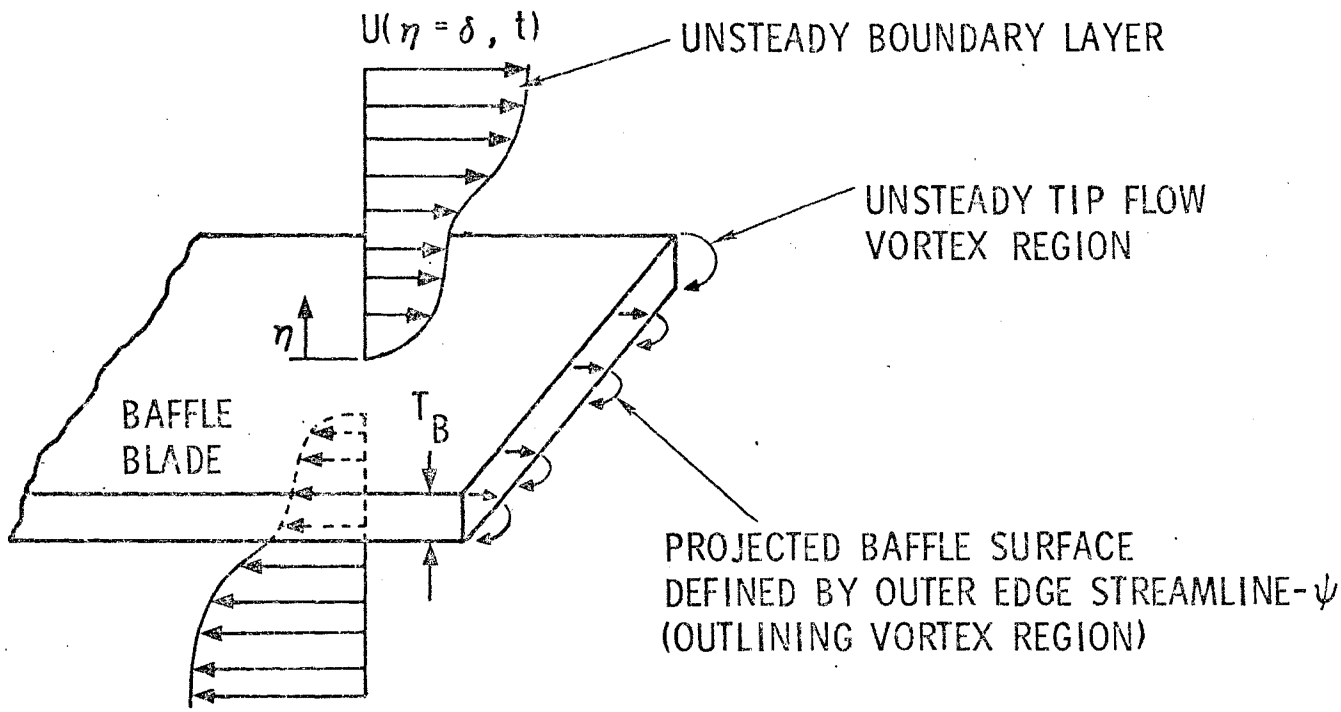
U(η = δ , t)
UNSTEADY BOUNDARY LAYER
UNSTEADY TIP FLOW
VORTEX REGION
η
BAFFLE
BLADE
T_B
PROJECTED BAFFLE SURFACE
DEFINED BY OUTER EDGE STREAMLINE-ψ
(OUTLINING VORTEX REGION)

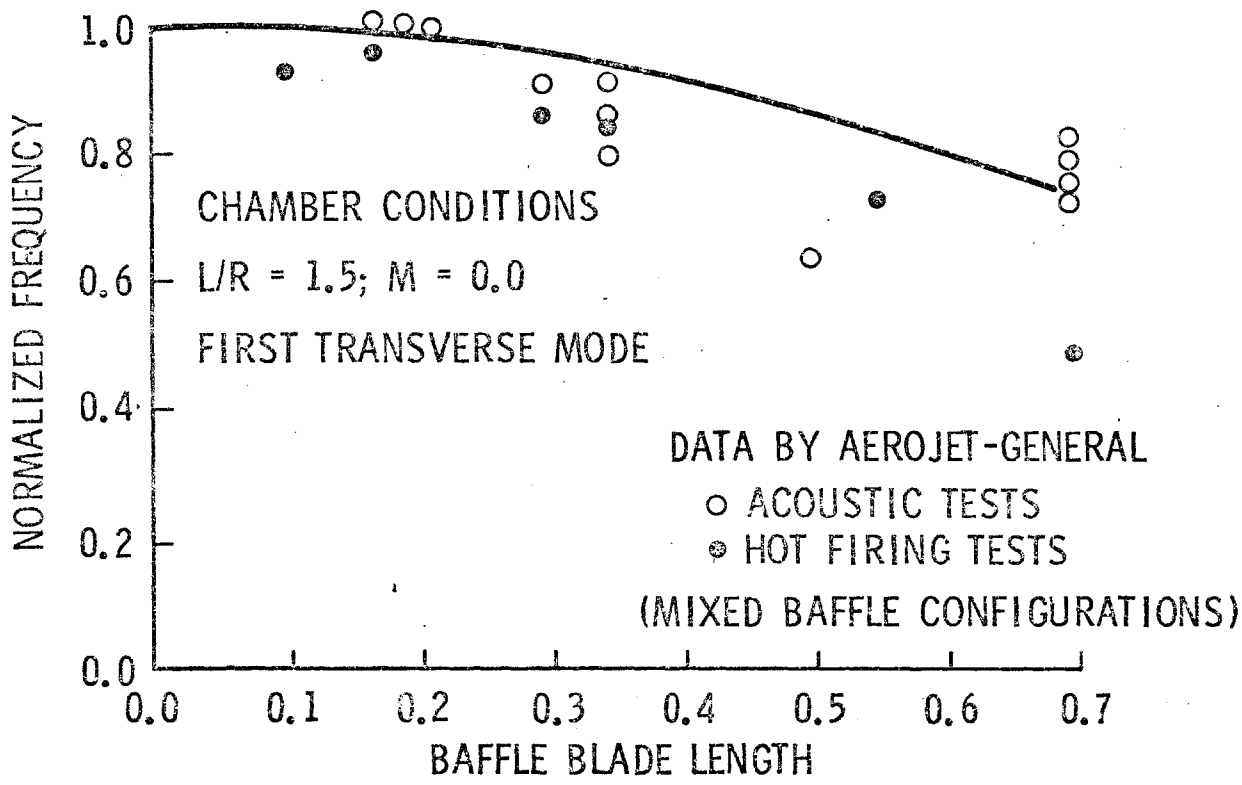
NORMALIZED FREQUENCY
1.0
0.8
0.6
0.4
0.2
0.0
CHAMBER CONDITIONS
L/R = 1.5; M = 0.0
FIRST TRANSVERSE MODE
DATA BY AEROJET-GENERAL
ACOUSTIC TESTS
HOT FIRING TESTS
(MIXED BAFFLE CONFIGURATIONS)
0.0
0.1
0.2
0.3
0.4
0.5
0.6
0.7
BAFFLE BLADE LENGTH

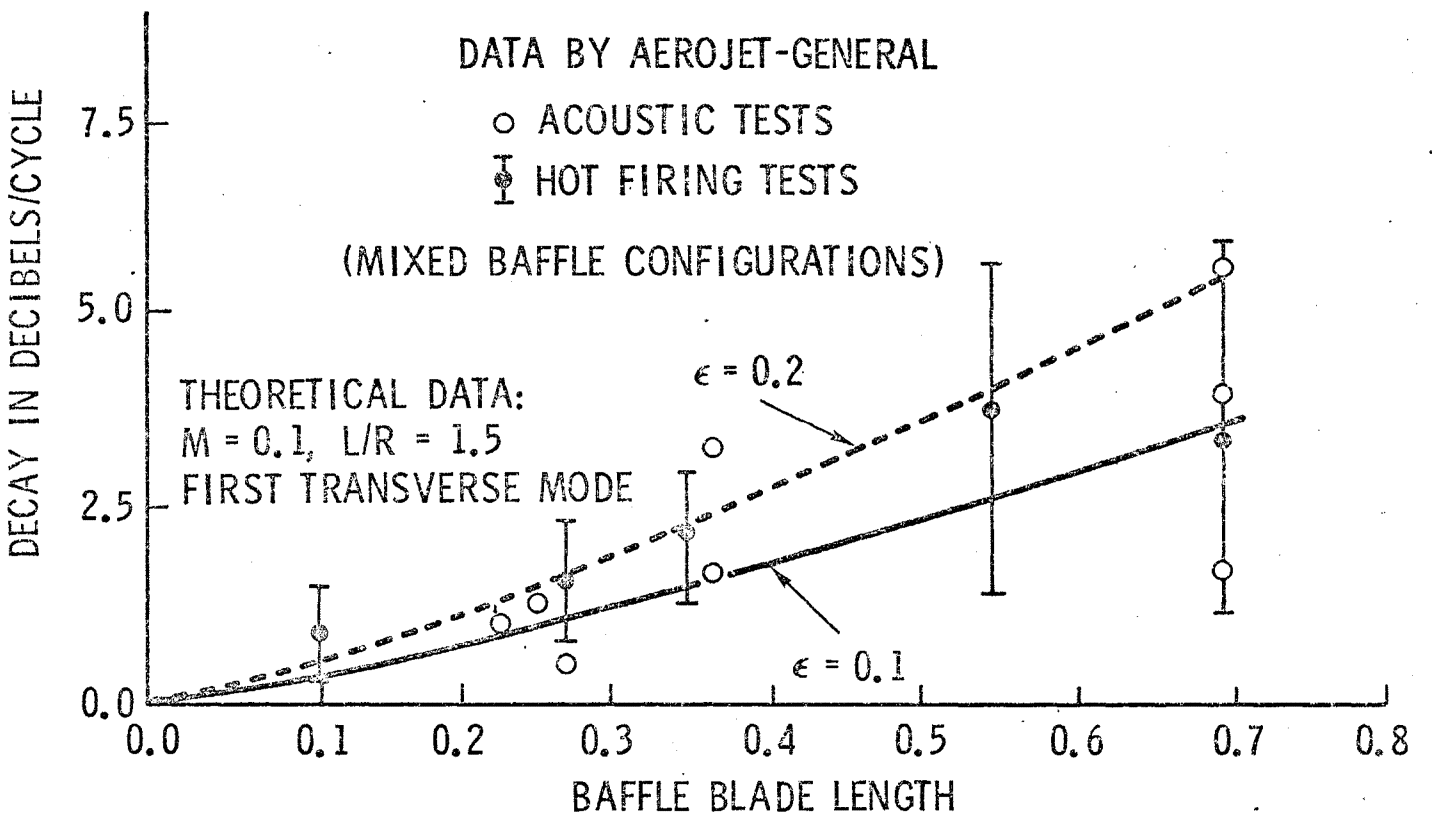
DATA BY AEROJET-GENERAL
ACOUSTIC TESTS
HOT FIRING TESTS
(MIXED BAFFLE CONFIGURATIONS)
THEORETICAL DATA:
M = 0.1, L/R = 1.5
FIRST TRANSVERSE MODE
ε = 0.2
ε = 0.1
DECAY IN DECIBELS/CYCLE
7.5
5.0
2.5
0.0
0.0
0.1
0.2
0.3
0.4
0.5
0.6
0.7
0.8
BAFFLE BLADE LENGTH

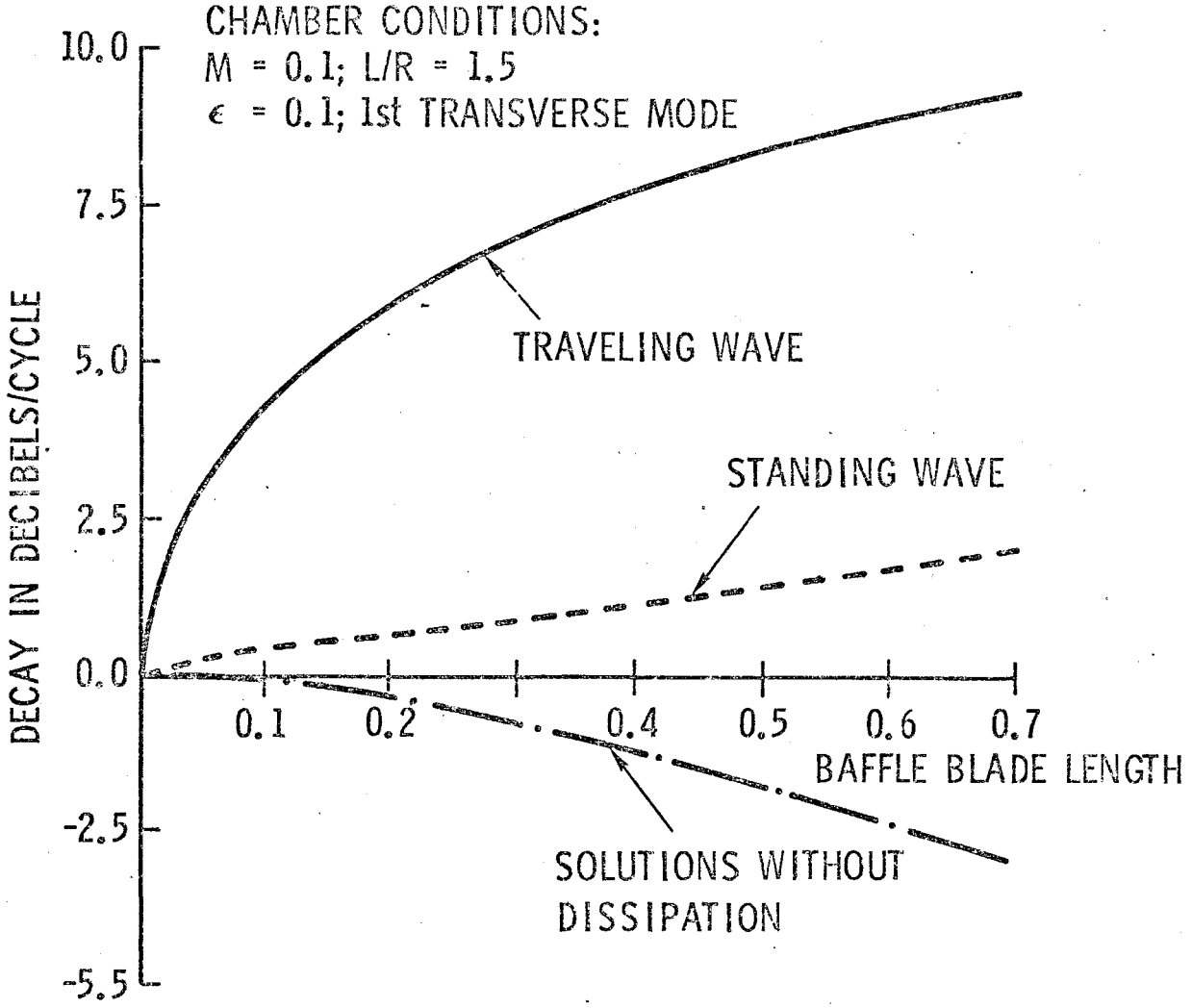
CHAMBER CONDITIONS:
M = 0.1; L/R = 1.5
ϵ = 0.1; 1st TRANSVERSE MODE
10.0
7.5
5.0
2.5
0.0
-2.5
-5.5
DECAY IN DECIBELS/CYCLE
TRAVELING WAVE
STANDING WAVE
SOLUTIONS WITHOUT DISSIPATION
0.1
0.2
0.4
0.5
0.6
0.7
BAFFLE BLADE LENGTH

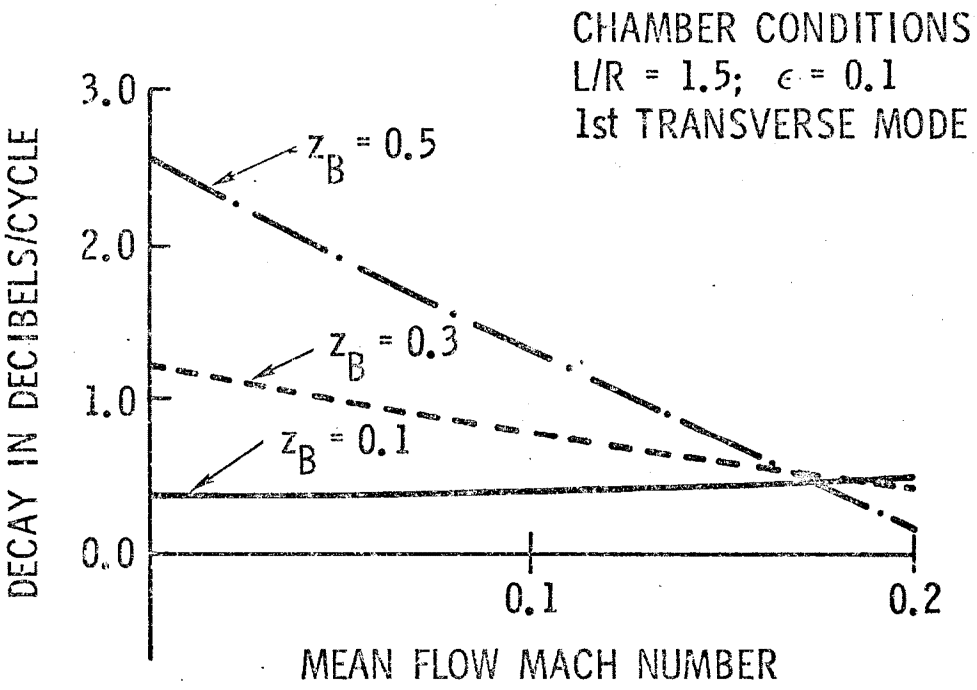
CHAMBER CONDITIONS
L/R = 1.5; ϵ = 0.1
1st TRANSVERSE MODE
DECAY IN DECIBELS/CYCLE
3.0
2.0
1.0
0.0
z_B = 0.5
z_B = 0.3
z_B = 0.1
0.1
0.2
MEAN FLOW MACH NUMBER

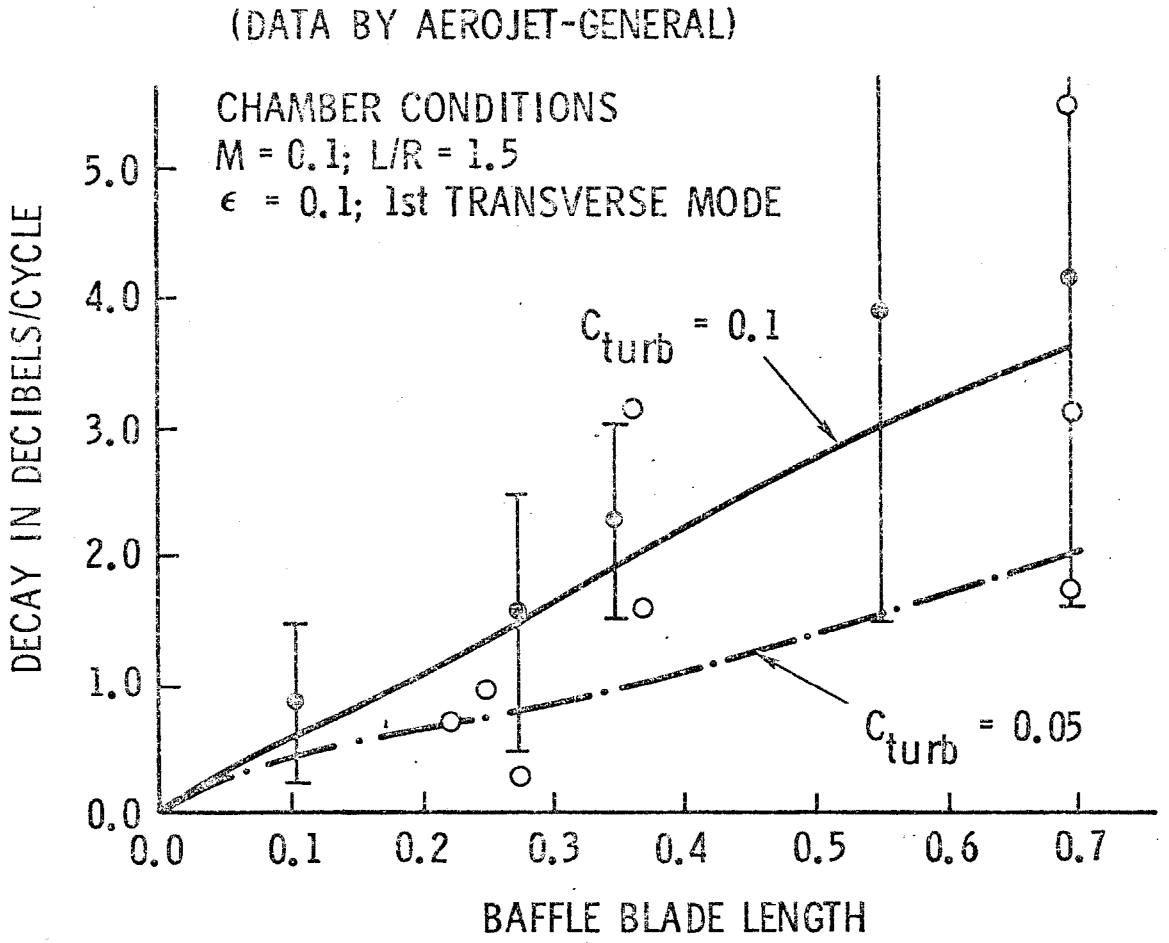
(DATA BY AEROJET-GENERAL)
CHAMBER CONDITIONS
M = 0.1; L/R = 1.5
ϵ = 0.1; 1st TRANSVERSE MODE
C_{turb} = 0.1
C_{turb} = 0.05
DECAY IN DECIBELS/CYCLE
BAFFLE BLADE LENGTH
0.0
1.0
2.0
3.0
4.0
5.0
0.0
0.1
0.2
0.3
0.4
0.5
0.6
0.7